International Journal of Heat and Mass Transfer 51 (2008) 6063–6076

Contents lists available at ScienceDirect

International Journal of Heat and Mass Transfer

journal homepage: www.elsevier.com/locate/ijhmt

Reduced order modeling and experimental validation of steady turbulent convection in connected domains

Qihong Nie, Yogendra Joshi *

G.W. Woodruff School of Mechanical Engineering, Georgia Institute of Technology, Atlanta, GA 30332, United States

ARTICLE INFO

Article history:
Received 5 September 2007
Received in revised form 30 April 2008
Available online 23 July 2008

Keywords:
Reduced order modeling
Multi-scale
Proper orthogonal decomposition
Flow network modeling
Server cabinet

ABSTRACT

The characterization and design of complex thermo/fluid electronics systems such as electronic racks requires attention to multiple length scales and transport phenomena, including conduction at the chip package level and convection at rack level. Detailed numerical calculations or experimental measurements are often time consuming and computationally expensive or simply infeasible. An efficient strategy to bridge length scales in multi-scale characterization is presented. Reduced order models for various system components obtained using proper orthogonal decomposition (POD) are assembled to model the complete system through flow network modeling (FNM). Boundary profile capturing capability at the interfaces of components is incorporated into the flux matching based POD approach, without introducing extra computation. The simulation errors of the component reduced order models are within 7.4% for temperature, velocity and pressure fields, compared to full-field computational simulations. Assembled component models result in a 12% error norm at the system level. Experimental validation with a representative electronic cabinet shows a difference of less than 10% in chip junction temperatures prediction.

1. Introduction

Fluid and thermal transport processes occur across multiple length scales in thermal management of electronic systems [1,2]. Characterization and modeling of these multi-scale systems are challenging and often impractical because each system may contain a variety of different subsystems and each subsystem may contain different electronic components. The number of degrees of freedoms (DOF) of such a system may be too large to be resolved by existing computational techniques and hardware. One strategy to bridge length scales is to develop separate models for individual components and assemble them to model the complete system [3,4]. Various levels of description for different components can be achieved. Modularization of individual subsystem models affords the ability to quickly integrate components into a new system model, without developing a new computational grid for altering the subcomponent models.

Each component or subsystem in a complex thermal fluid system may still have millions of DOF, rendering a full computational fluid dynamics and heat transfer (CFD/HT) model inefficient and even infeasible. This motivates a reduced order modeling methodology where the number of DOF is significantly reduced, producing modeling accuracy acceptable for engineering design and optimization. The proper orthogonal decomposition (POD) is increasingly being used as a promising solution for reduced order modeling of non-linear phenomena [5–23], owing to its stochastic nature of the subspace calculation.

One key concern in the existing POD methodology is determining the weighted coefficients for the POD modes required to construct a POD subspace that faithfully represents the physics of the system. The standard method of evaluating the weight coefficients for each POD mode is to project the governing equations onto the modal subspace, known as the Galerkin method or Galerkin projection [5–21]. One major limitation of the traditional method is that it is only applicable to configurations with homogeneous boundary conditions. For inhomogeneous boundary conditions, some authors [12–16] homogenize the boundary conditions by introducing a reference field to eliminate the need for boundary pressure–velocity coupling. This approach may require full numerical computations for each new set of boundary conditions. To avoid this limit, Ly and Tran [19] proposed a simple approximation method based on interpolating splines between weight coefficients to match a desired parameter value. This method would require higher order multi-dimensional interpolation to model a complex system with multiple parameters and also does not guarantee that the desired parameter level will be achieved. A flux matching approach was proposed by Rambo et al. [22,23], which enforces the POD modes to satisfy the flux or its integral condition such as mass or heat flow rate at the boundaries. This technique overcomes the limits of both Galerkin projection method and coefficients interpolation method. However,

* Corresponding author. Tel.: +1 404 385 2810; fax: +1 404 894 8496.
E-mail addresses: qhnie@me.gatech.edu (Q. Nie), yogendra.joshi@me.gatech.edu (Y. Joshi).

0017-9310/$ - see front matter © 2008 Elsevier Ltd. All rights reserved.
doi:10.1016/j.ijheatmasstransfer.2008.04.068

Nomenclature

a, b, c	modal coefficients
$\boldsymbol{a}$, $\boldsymbol{b}$, $\boldsymbol{c}$	modal coefficients matrix
A	cross-sectional area, m^2
c_p	specific heat, J/kg K
c_μ	k–ε model coefficient
E	eigenvalue energy spectra
F	flow rate function
G	goal flow rate function
H^2	Hilbert space
K	pressure loss coefficient
$\mathbf{n}$	normal direction
$\mathbf{P}$, $\mathbf{T}$, $\mathbf{U}$	observation ensemble matrix
P	pressure, N/m^2
Pr_t	turbulence Prandtl number
Q	heat generation, W
r	correlation coefficient
R	subspace of Hilbert space
Re_L	Reynolds number
S	momentum source term
T	temperature, K
$\mathbf{u}$	velocity field, m/s
u	horizontal velocity, m/s
U	ensemble matrix
V	flow field variables, P, T, $\mathbf{u}$

Greek symbols

Γ	boundary
κ	thermal conductivity, W/m K
λ	eigenvalue
ν	kinetic viscosity, m^2/s
Π, Φ, Ψ	POD modal space
ρ	density, kg/m^3
φ, ϕ, ψ	POD mode
Ω	system domain

Subscripts

c	constant part of source term
eff	effective fluid property
err	error
h	heat flow
m	mass flow
o	source
p	slope of source term

Superscripts

m	number of nodes
n	number of modes
obs	observations
r	reconstructed solution
s	number of complement modes
t	desired solution
T	transpose
$'$	complement subspace
–	matrix inverse
$\perp$	orthogonal subspace
+	pseudo-inverse

the flux matching could be a problem when modeling multiple interconnected subsystems, where the system variables at the interface usually have non-uniform profiles. Replacing the non-uniform boundary conditions with a constant, representing an integrated constraint may result in serious simulation errors. Therefore, it is necessary to develop a new method to overcome this limit.

In this paper, an innovative boundary profile based flux matching POD reduced order modeling methodology is developed for thermal/fluids characterization of electronic systems, by utilizing the flow network modeling (FNM) approach [24–26] to interconnect multiple subsystems. The method is essentially based on the unique mapping among the mass flow rate and pressure or velocity profile at the boundaries. POD generates the full domain solution for each subsystem so that the momentum equation and mass and energy conservation equations can be obtained for each link or channel, which are used in FNM to achieve order reduction at system level. The methodology is subsequently validated by comparisons with experiments on a test bed.

2. Proper orthogonal decomposition (POD)

We begin by giving an overview of the POD framework for reduced order modeling in this section. Consider a three-dimensional steady incompressible turbulent flow with negligible buoyancy effects. The Reynolds averaged Navier–Stokes (RANS) continuity, momentum and energy equations are

$$\nabla \cdot \mathbf{u} = 0 \tag{1a}$$

$$\mathbf{u} \cdot \nabla \mathbf{u} - \nabla \cdot (\nu_{\text{eff}} \nabla \mathbf{u}) + \frac{1}{\rho} \nabla P = 0 \tag{1b}$$

$$\rho c_p \mathbf{u} \cdot \nabla T - \nabla \cdot (\kappa_{\text{eff}} \nabla T) = 0 \tag{1c}$$

where $\nu_{\text{eff}} = \nu + c_\mu \frac{k^2}{\varepsilon}$ and $\kappa_{\text{eff}} = \kappa + \frac{c_p \nu_t}{\rho Pr_t}$ with $Pr_t = 0.85$ and can be computed through any RANS-based turbulence model and non-equilibrium wall functions [27]. For now, assume we have a reduced-basis of dimension n, $\{\varphi_i(\cdot)\}_{i=1}^n$ with $\varphi_i(\cdot) \in H^2(\Omega)$. With this basis, the reduced order approximation to the velocity vector $\mathbf{u}$ is represented as

$$\mathbf{u}^r = \sum_{k=1}^{r} a_k \varphi_k, \quad r \leqslant n \tag{2}$$

where the modes $\varphi_k(x)$ can be obtained through the method of snapshots [10]

$$\varphi_k = \sum_{i=1}^{n} \alpha_{k,i} \mathbf{u}_i \tag{3}$$

and the weight coefficients matrix $\{\alpha_{k,i}\}_{i,k=1}^n$ here are eigenvectors of the solution to

$$D\varphi(x) = \lambda\varphi \tag{4}$$

where $D = \mathbf{U}^T\mathbf{U}/n \in R^{n\times n}$ with $\mathbf{U} = \{\mathbf{u}_1, \mathbf{u}_2, \ldots, \mathbf{u}_n\} \in R^{m\times n}$. The coefficients a_k in Eq. (2) are typically solved by Galerkin projection method, which projects the governing Eqs. (1a) and (1b) into the space spanned by the POD modes $\varphi_k(\vec{x})$

$$(\nabla \cdot \mathbf{u}^r, \varphi_k) = 0 \tag{5}$$

$$(\mathbf{u}^r \cdot \nabla \mathbf{u}^r, \varphi_k) - (\nabla \cdot (\nu_{\text{eff}} \nabla \mathbf{u}^r), \varphi_k) + \frac{1}{\rho}(\nabla P, \varphi_k) = 0 \tag{6}$$

However, homogenization of boundary conditions is required with this method to eliminate the need for velocity and pressure or temperature coupling at the boundaries. A flux function, usually given as an integral condition such as mass flow rate, is defined on the boundary [22,23]

$$F_{\mathrm{m}}(\mathbf{u}) = \int_{\Gamma_{\mathrm{m}}} \rho \mathbf{u} \cdot \mathbf{n} \mathrm{d}A, \quad \Gamma_{\mathrm{m}} \subseteq \Omega \tag{7}$$

The goal is to fit the POD modes to match a goal flux function $G_{\mathrm{m}} = F_{\mathrm{m}}(\mathbf{u}^{\mathrm{r}})$ corresponding to the reduced order velocity vector by solving the following least squares problem:

$$\min \left\{ \left\| G_{\mathrm{m}} - \sum_{k=1}^{r} a_k F_{\mathrm{m}}(\varphi_k) \right\| \right\} \tag{8}$$

The weighted coefficient vector $\mathbf{a} = \{a_k\}_{k=1}^{r}$ here can be computed as

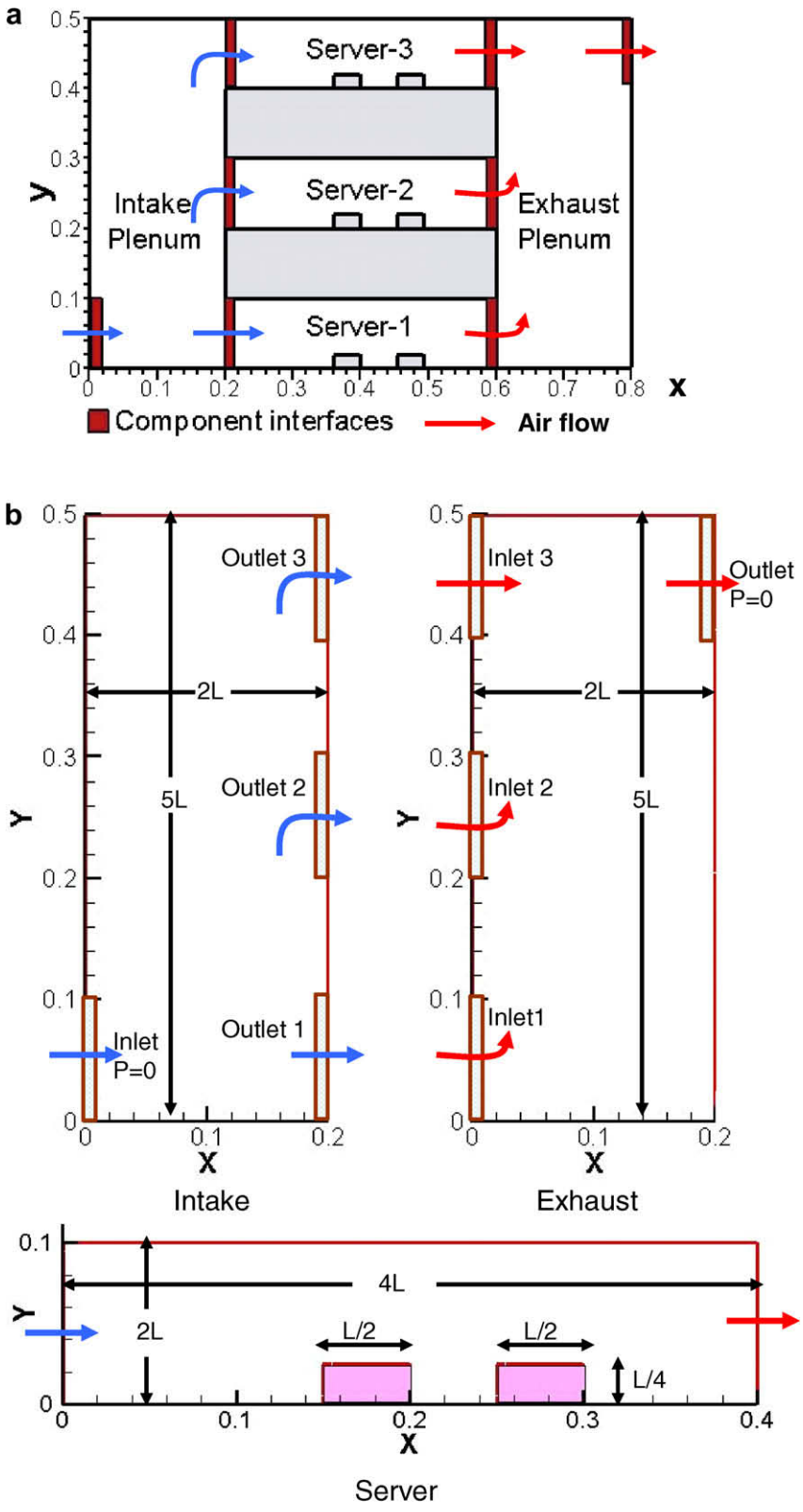

Fig. 1. Two-dimensional rack model [1]: (a) system model and (b) geometry of components.

$$\mathbf{a} = F_{\mathrm{m}}^{+}(\Phi)G_{\mathrm{m}}(\mathbf{u}^{\mathrm{r}}) \tag{9}$$

where $F^{+} = (F^{\mathrm{T}}F)^{-1}F^{\mathrm{T}}$ is the Moore–Penrose matrix pseudo-inverse producing the least squares approximation, and $\Phi = \{\varphi_1, \varphi_2, \ldots, \varphi_n\}$.

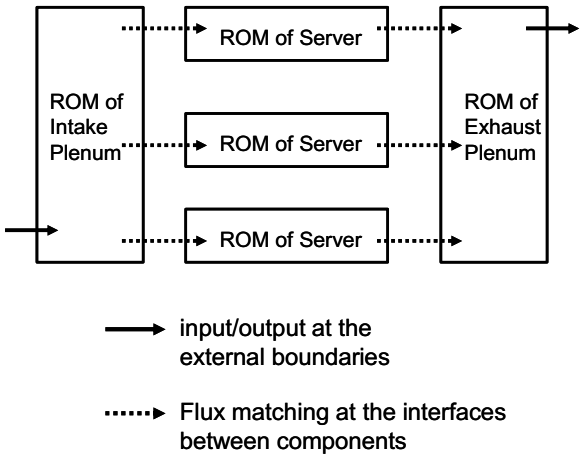

Fig. 2. Reduced order modeling methodology.

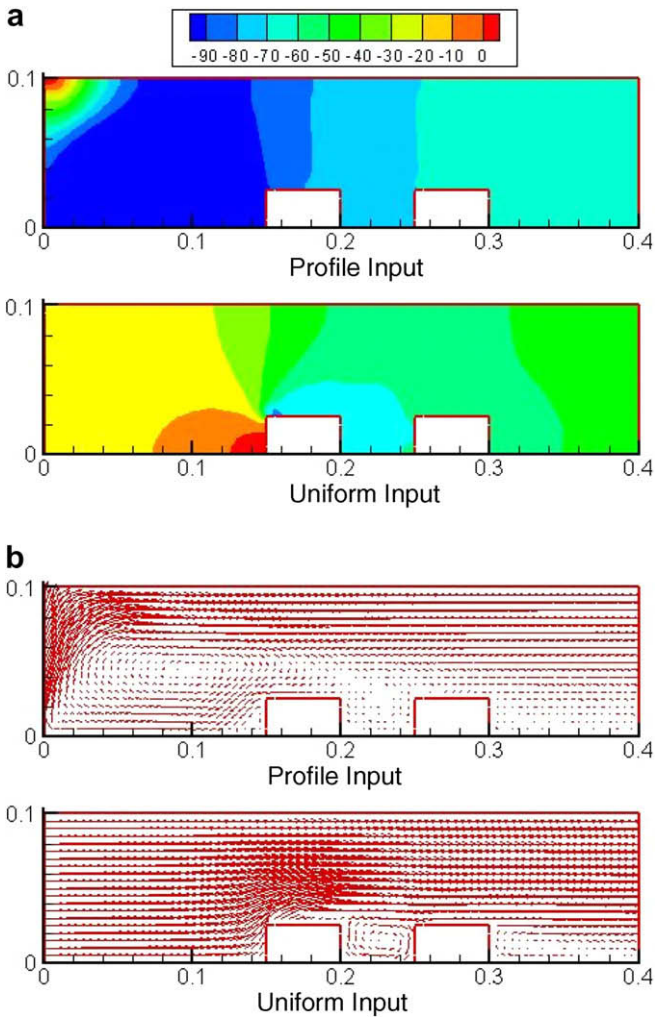

Fig. 3. Comparison of profile input and uniform input: (a) pressure field (Pa) and (b) velocity field.

To alleviate the poor approximations for solutions far from the system reference point in parameter dependent flows, a weighted POD was proposed in [28] by pre-weighting certain modes to increase their contribution on the superposition. One concern with this method lies in the fact that weighting is not unique and additional information about which modes to weight is required. Furthermore, the POD subspace is collapsed to a point near that single observation or snapshot as its weighting factor increases. To solve these problems, a complimentary POD (PODc) or pre-defined POD (p-POD) was described in [23,28], which decomposes the POD subspace into orthogonal complement subspaces

$$\Phi = \varphi^{\perp} + \varphi', \quad \text{where } \varphi^{\perp} \in R^{n\times s} \quad \text{and} \quad \varphi' \in R^{n\times r-s} \tag{10}$$

The orthogonal complement set $\varphi^{\perp}$ is chosen to best satisfy the inhomogeneous boundary conditions and φ' describes the flow features over the rest of the POD domain. For instance, the two snapshots ($s = 2$) whose boundary conditions are closest to the test boundary condition can be used to construct $\varphi^{\perp}$, and the rest of the snapshots for φ'. The modal expansion and minimization problem are modified to

$$\mathbf{u}^{\mathrm{r}} = \mathbf{u}_{\mathrm{o}} + \sum_{k=1}^{r} a_k\varphi_k, \quad \varphi_k \in \Phi = \{\varphi^{\perp}, \varphi'\} \tag{11}$$

$$\min\left\{\left\|G_{\mathrm{m}} - F_{\mathrm{m}}(\mathbf{u}_{\mathrm{o}}) - \sum_{k=1}^{r} a_k F_{\mathrm{m}}(\varphi_k)\right\|\right\} \tag{12}$$

where $\mathbf{u}_{\mathrm{o}}$ represents the source function for velocity.

The flux matching procedure (FMP) can be extended to include the energy equation, accordingly the heat flux function can be defined analogous to (5) as

$$F_{\mathrm{h}}(T) = \int_{\Gamma_{\mathrm{h}}} k\nabla T\cdot\mathbf{n}\mathrm{d}A, \quad \Gamma_{\mathrm{h}} \subseteq \Omega \tag{13}$$

The heat flux control surfaces are typically defined at the three surfaces of each heating component or the inlet of a flow domain. Since temperature field depends on the velocity field, the temperature complementary POD subspace $\phi^{\perp}$ is constructed with the snapshot whose velocity boundary condition is closest to the test velocity

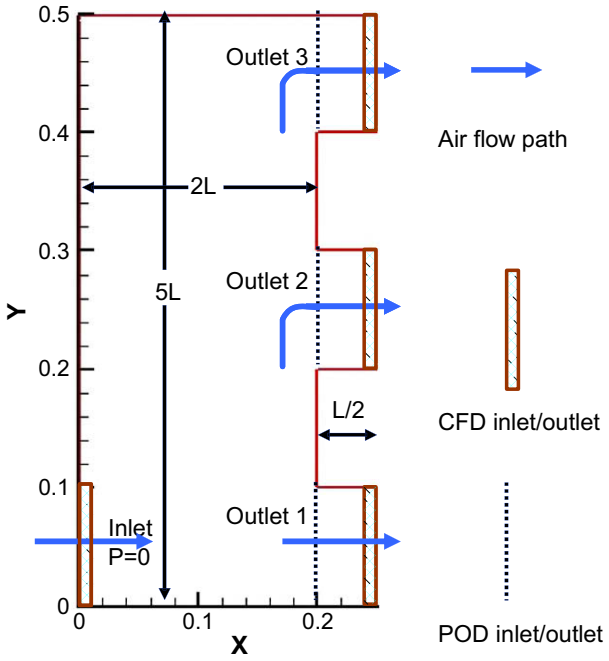

Fig. 4. Flow straightening duct.

boundary condition. Additionally, multiple snapshots closest to the test temperature boundary conditions are selected. Similarly, the temperature solution can be approximated by

$$T^{\mathrm{r}} = T_{\mathrm{o}} + \sum_{k=1}^{r} b_k \phi_k, \quad \phi_k \in \Psi = \{\phi^{\perp}, \phi'\} \tag{14}$$

where T_{o} is the temperature source term. The modal coefficients vector $\mathbf{b} = \{b_k\}_{k=1}^{r}$ in Eq. (14) can be obtained by solving the following optimization problem:

$$\min\left\{\left\| G_{\mathrm{h}} - F_{\mathrm{h}}(T_{\mathrm{o}}) - \sum_{k=1}^{r} b_k F_{\mathrm{h}}(\phi_k)\right\|\right\} \tag{15}$$

Since many flows in electronic systems are pressure-driven, such as fans moving air through a series of channels, it is necessary to calculate the pressure field. However, one property of POD analysis is the elimination of pressure for incompressible flow. In theory, the flux matching technique can be extended to include the pressure term if the pressure boundary conditions are known. However, only boundary velocity or flow rate is available for many thermal fluids systems. The response surface methodology can be used to deal with this case [1], where the pressure POD modes are projected back onto the pressure observations ensemble $\mathbf{P} = \{P_1, P_2, \ldots, P_n\}$ to obtain the set of observation weight coefficients

$$\mathbf{c}^{\mathrm{obs}} = \Pi^{+}\mathbf{P} \in R^{n\times n} \tag{16}$$

where $\Pi = \{\psi_1, \psi_2, \ldots, \psi_n\}$ is the pressure modal subspace. A n-dimensional quadratic response surface of the form $\mathbf{c}^{\mathrm{obs}} = f(G_{\mathrm{m}}^{\mathrm{obs}})$ is computed for the pressure modes as a function of the observational mass fluxes, $G_{\mathrm{m}}^{\mathrm{obs}}$. The weight coefficients for pressure modes corresponding to the desired mass flow rate $G_{\mathrm{m}}^{\mathrm{t}}$ are then evaluated as $\mathbf{c} = f(G_{\mathrm{m}}^{\mathrm{t}}) = \{c_k\}_{k=1}^{r}$ and the approximate pressure field is assembled as

$$P^{\mathrm{r}} = \sum_{k=1}^{r} c_k \psi_k \tag{17}$$

The energy captured by each POD mode is computed as $E_i = \lambda_i / \sum_{k=1}^{n} \lambda_k$ and the total energy resolved using the first r modes is $E^{\mathrm{r}} = \sum_{k=1}^{r} \lambda_k / \sum_{k=1}^{n} \lambda_k$, where λ_k are the eigenvalues of $(1/n)U^{\mathrm{T}}U \in R^{n\times n}$ with $U = \mathbf{U}$, $\mathbf{T}(=\{T_1, T_2, \ldots, T_n\})$, and $\mathbf{P}$ for velocity, temperature, and pressure observation assembly, respectively.

Table 1
Intake plenum flow observations, ΔP (Pa) and $\dot{m}$ (kg/s)

k	Outlet 1		Outlet 2		Outlet 3	
	ΔP_1	$\dot{m}_1$	ΔP_2	$\dot{m}_2$	ΔP_3	$\dot{m}_3$
1	1.8	0.185	11.4	0.135	12.0	0.136
2	3.5	0.258	22.9	0.189	23.4	0.191
3	5.7	0.332	37.9	0.243	38.9	0.246
4	8.4	0.406	57.1	0.297	57.1	0.301
5	11.6	0.479	78.8	0.350	81.2	0.356
6	15.2	0.553	104.3	0.405	109.4	0.411
Test	10.4	0.461	70.9	0.337	73.8	0.342

Table 2
Server flow observations, ΔP (Pa), $\dot{m}$ (kg/s) and Q (W)

k	Server 1			Server 2			Server 3		
	ΔP_1	$\dot{m}_1$	Q_1	ΔP_2	$\dot{m}_2$	Q_2	ΔP_3	$\dot{m}_3$	Q_3
1	0.54	0.185	60	−1.41	0.135	45	−0.15	0.136	50
2	1.10	0.258	75	−2.72	0.189	60	−0.37	0.191	65
3	1.83	0.332	90	−4.70	0.243	75	−0.68	0.246	80
4	2.67	0.406	105	−7.14	0.297	90	−1.07	0.301	95
5	3.65	0.479	120	−9.69	0.350	105	−1.54	0.356	110
6	4.80	0.553	135	−12.71	0.405	120	−2.01	0.411	125
Test	3.26	0.461	110	−9.23	0.337	110	−1.42	0.342	90

Table 3
Exhaust plenum flow observations, ΔP (Pa) and $\dot{m}$ (kg/s)

k	Outlet 1		Outlet 2		Outlet 3	
	ΔP_1	$\dot{m}_1$	ΔP_2	$\dot{m}_2$	ΔP_3	$\dot{m}_3$
1	16.5	0.185	14.9	0.135	13.4	0.136
2	32.7	0.258	29.0	0.189	26.3	0.191
3	53.9	0.332	48.7	0.243	43.7	0.246
4	80.1	0.406	73.1	0.297	65.6	0.301
5	112.9	0.479	102.7	0.350	91.4	0.356
6	150.2	0.553	136.8	0.405	121.9	0.411
Test	104.8	0.461	95.2	0.337	84.6	0.342

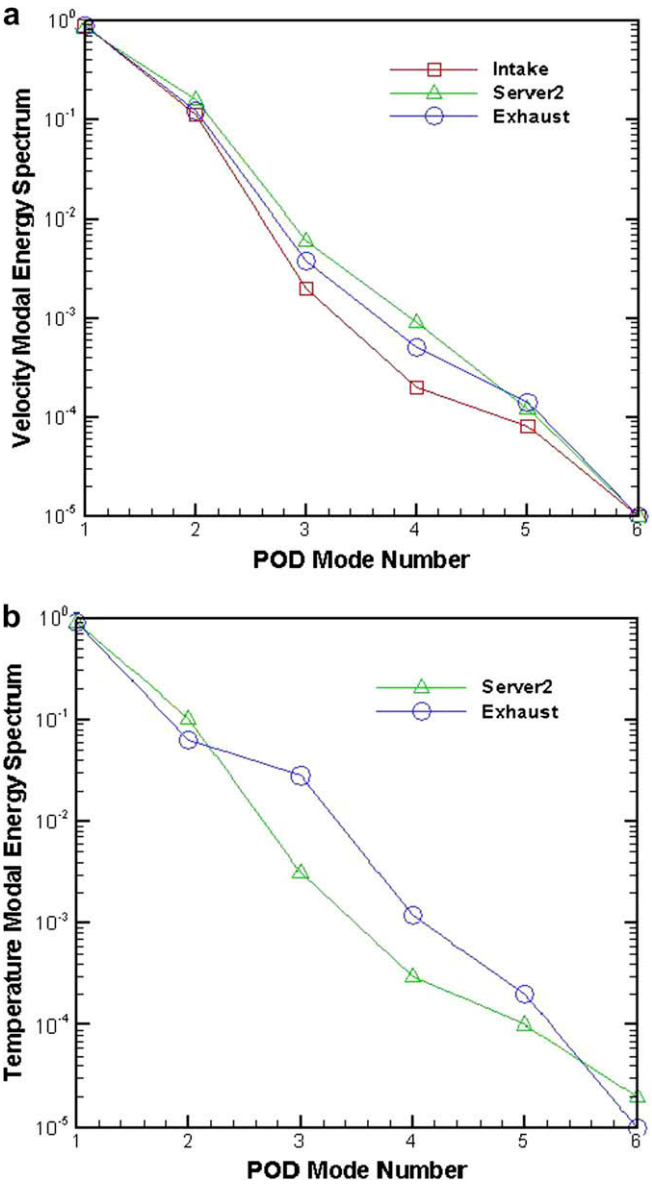

Fig. 5. Modal spectra for the POD procedure: (a) velocity and (b) temperature.

3. Reduced order modeling for interconnected multi-scale domains

Many electronics systems such as electronics cabinets are modular in nature, consisting of a series of nested sub-domains. Fig. 1 shows such an example, a highly simplified 2-dimensional model of an air-cooled rack containing multiple servers and two plena at the intake and exhaust [1]. The general approach here is to divide such system into multiple sub-domains or subsystems. A POD based reduced order model (ROM) with input and output information is constructed for each subsystem separately and subsequently linked together to model the complete system, as shown in Fig. 2 for the demonstrated example. However, inputs and outputs (boundary conditions) of thermal fluid systems are generally unknown profiles, instead of fixed variables, which make the development of ROM for each subsystem and their handshaking of ROMs challenging. A general approach to overcome this limitation is to replace the profile inputs/outputs with their averages [1]. However, large errors may be incurred with this approach. Consider a server model shown in Fig. 1. Two simulations are conducted with two different boundary conditions but same average mass flow rate at the inlet of the server. All other boundary conditions remain the same for both cases. The flow and pressure fields of two cases are quiet different from Fig. 3, which indicates that the effect of the boundary profile is not negligible.

A typical way to capture the boundary profile is to utilize the output profiles of the sub-domain upstream as the inlet boundary profiles of sub-domain downstream. However, large errors may be incurred, since the sub-domains downstream may affect the flow pattern of the fluid at the exits of sub-domain upstream. To keep

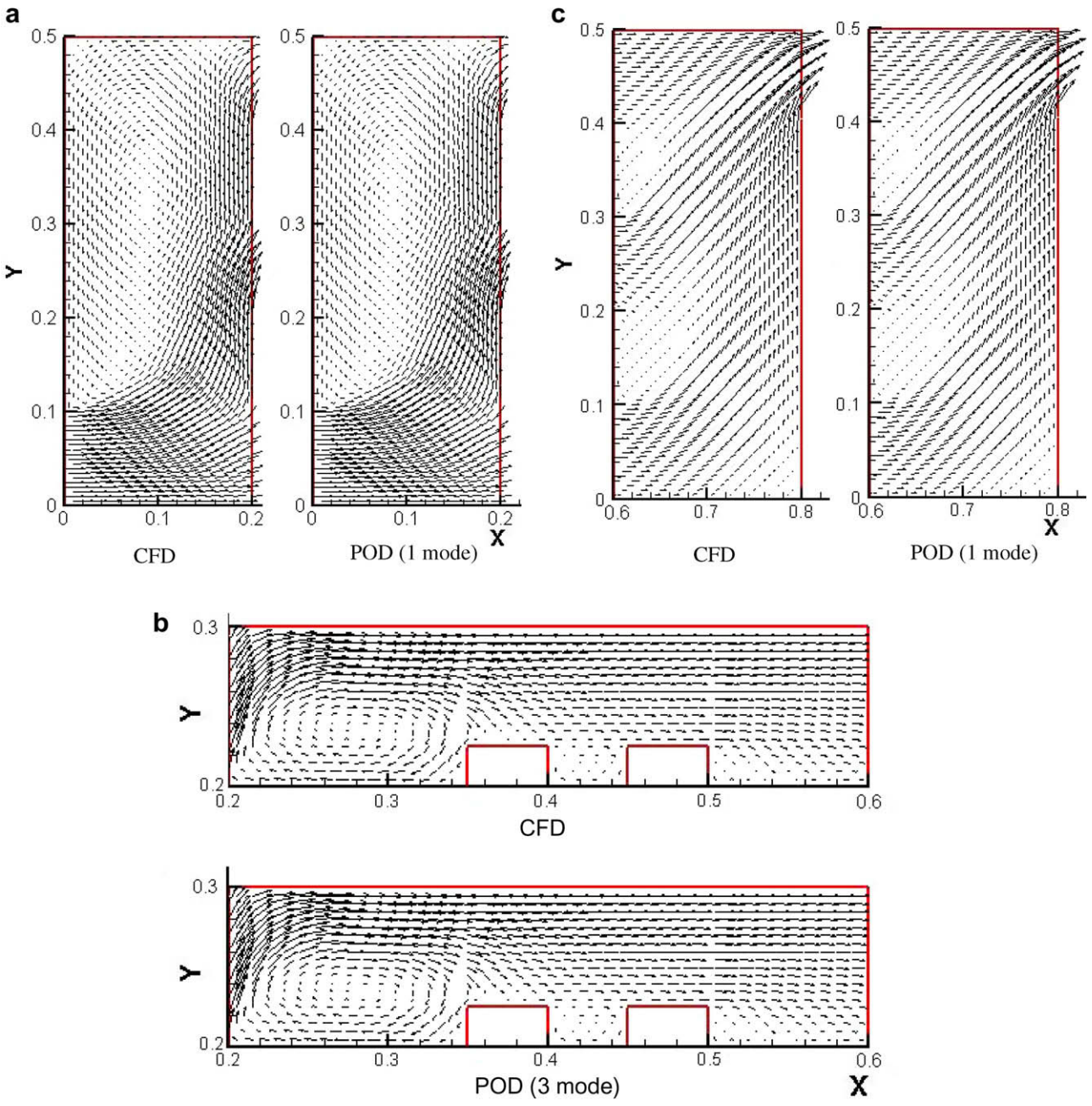

Fig. 6. Velocity comparison of CFD and POD simulation results: (a) intake plenum, (b) server 2, and (c) exhaust plenum.

the flow pattern of the outputs of the sub-domain upstream close to the complete system, a flow straightening duct with the same cross-sectional geometry as the sub-domain downstream can be added to each outlet of the sub-domain upstream (see Fig. 4 for the demonstrated example). Since each boundary profile corresponds to a specific flow rate, the same flux matching POD technique can be used to construct the ROM for each sub-domain.

To assemble the full system with ROMs for the system components, concepts from FNM [24–26] are used to generate the matching conditions between the interfaces of those ROMs. Each system component is represented by a combination of links and nodes. Pressure and temperature are calculated at each node characterized by conservation law

$$\sum_i G_{m,i} = 0 \quad \text{and} \quad \sum_i G_{h,i} = 0 \tag{18}$$

for mass and energy, respectively, while the flow rates are associated with links characterized by the following momentum equation:

$$P_1 - P_2 = \Delta P = f(G_m) = K_1 G_m^2 + K_2 G_m \tag{19}$$

The pressure loss coefficient K_1 and K_2 here for standard components (screens, ducts, bends, etc.) can be found from handbooks or Moody chart [29]. For non-standard components, experimental data or CFD simulations can be used to get the flow characteristics. With POD method, CFD snapshots for each component can be used to obtain the flow characteristic of each component without introducing extra computational cost. A flow resistance network can be constructed with those links and nodes for the entire system. Linearization of Eq. (19) is necessary to solve this network [25]

$$P_1 - P_2 = \Delta P = S_c + S_p G_m \tag{20}$$

where

$$S_c = \left(1 - \left(\frac{d\Delta P}{dG_m}\right)^*\right) G_m^* \quad \text{and} \quad S_p = \left(\frac{d\Delta P}{dG_m}\right)^* \tag{21}$$

The '*' here represents the value at current iteration.

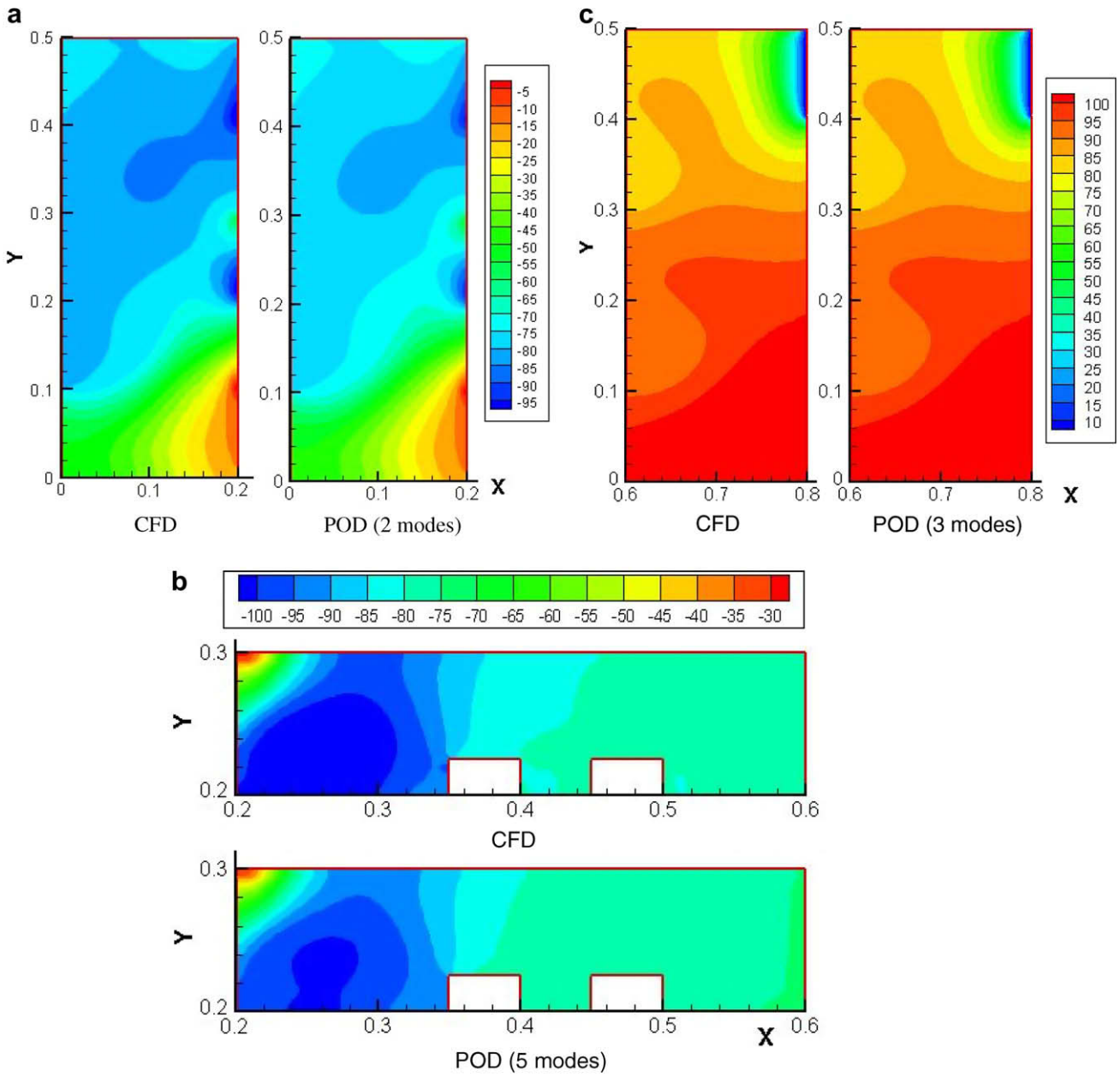

Fig. 7. Pressure (Pa) comparison of CFD and POD simulation results: (a) intake plenum, (b) server 2, and (c) exhaust plenum.

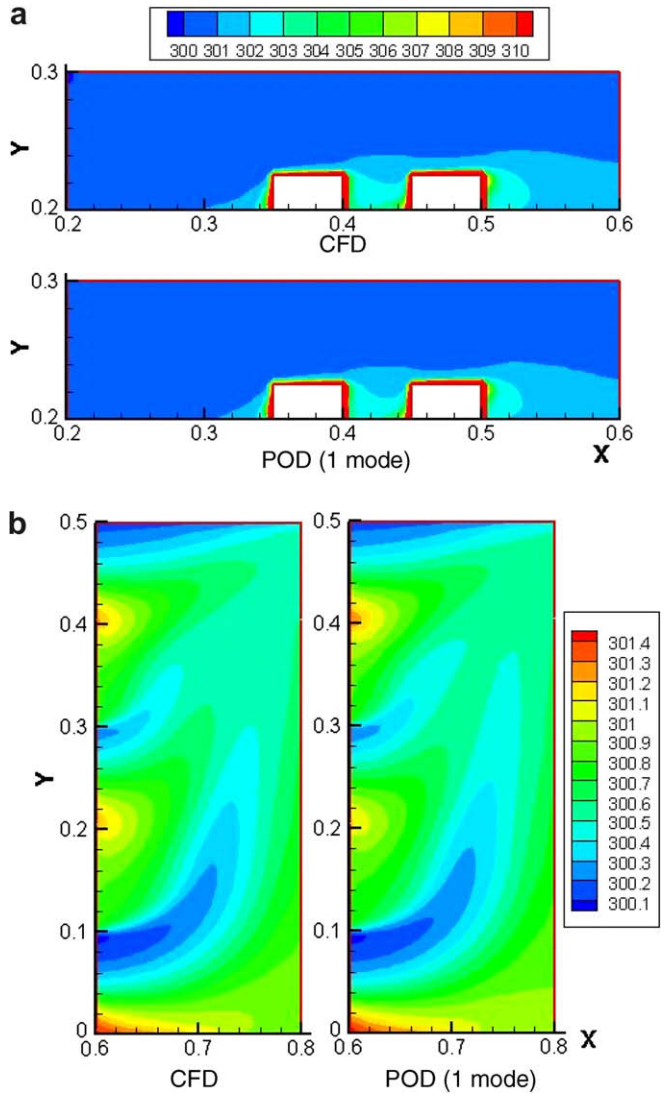

Fig. 8. Temperature (K) comparison of CFD and POD simulation results: (a) server 2, and (b) exhaust plenum.

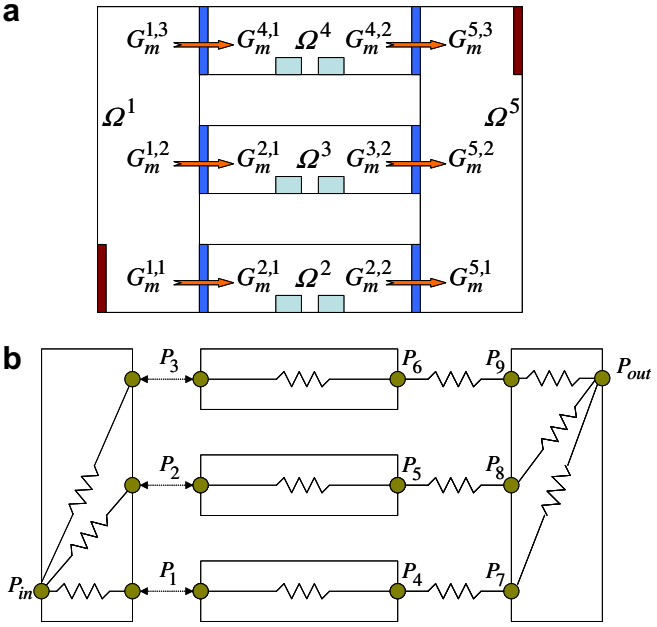

Fig. 9. FNM: (a) system nomenclature and (b) system flow resistance network.

pling methods in incompressible CFD and is outlined here with more details available in [30]:

FNM – SIMPLE algorithm:

(1) Assume a nodal pressure distribution and a link mass flow rate distribution.
(2) Use the momentum link equations $\Delta P = f(G_m)$ to calculate the momentum link flow rates given the nodal pressures.
(3) Construct a pressure correction equation by combining the corrected momentum and continuity equations. Solve the pressure correction matrix through direct method, and update the pressure and flow rates.
(4) Repeat steps 2 to 4 till convergence.
(5) Solve the velocity and temperature fields with POD, given the link flow rates and heat loads; solve the pressure fields with response surface method, given the link flow rates.

Table 4
POD modeling error norm (Error), %, and number of POD modes (#) used

	Intake		Server 1		Server 2		Server 3		Exhaust	
	#	Error	#	Error	#	Error	#	Error	#	Error
Velocity	1	2.1	4	0.7	3	0.9	1	2.5	1	0.4
Pressure	2	1.3	5	1.0	5	3.2	5	1.2	3	0.2
Temperature	NA	NA	1	5.6	1	7.4	1	7.0	1	7.2

The standard SIMPLE algorithm [25] is used to solve for the nodal pressure, momentum link flow rates and the energy flow rates. The procedure is completely analogous to pressure–velocity cou-

4. Computational case study

To demonstrate the methodology, consider the example model shown in Fig. 1. The intake and exhaust plena are symmetrical and both measure $2L \times 5L$, with $L = 0.1$ m. The flow straightening duct and server measure $L \times L/2$ and $4L \times L$, respectively, as shown in Fig. 1b. All models were developed for the range $7{,}290 \leqslant Re_L \leqslant 26{,}768$. Tables 1–3 list the observations used to construct the component ROMs. It is noted that the pressure boundary conditions are specified for intake plenum, whose flow is pressure driven. The velocity boundary conditions are specified at the inlet, and pressure boundary conditions at the outlet for both server and exhaust plenum.

Table 5
Pressure loss coefficients K_1, K_2 and r^2 (square of correlation coefficient) for each component

	Intake			Server 1	Server 2	Server 3	Exhaust		
	Outlet 1	Outlet 2	Outlet 3				Inlet 1	Inlet 2	Inlet 3
K_1	47.256	630.89	658.52	14.857	−76.43	−13.33	495.25	851.77	722.52
K_1	1.507	3.995	−5.951	0.531	−0.872	0.48	−2.324	−6.132	0.038
r^2	0.99983	0.99981	0.99884	0.99873	0.99845	0.99237	0.99848	0.99859	0.99951

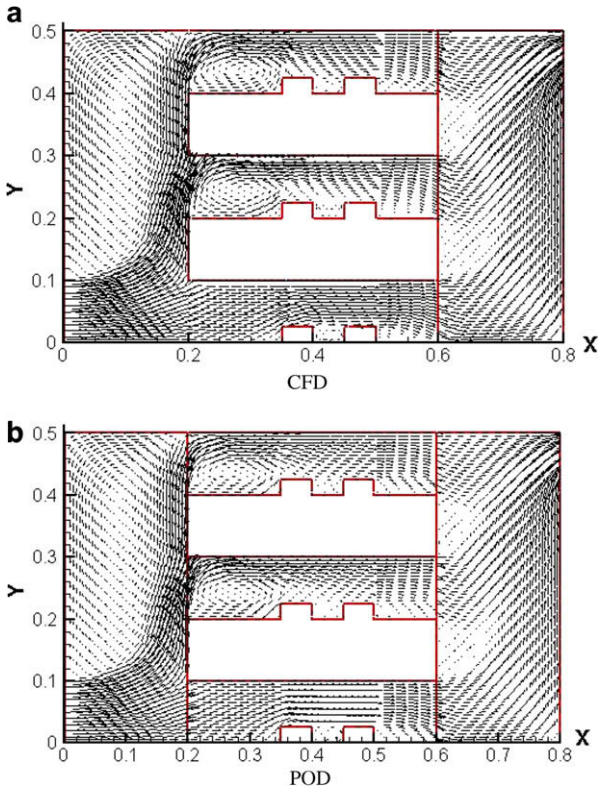

Fig. 10. Velocity comparison at system level: (a) CFD and (b) POD.

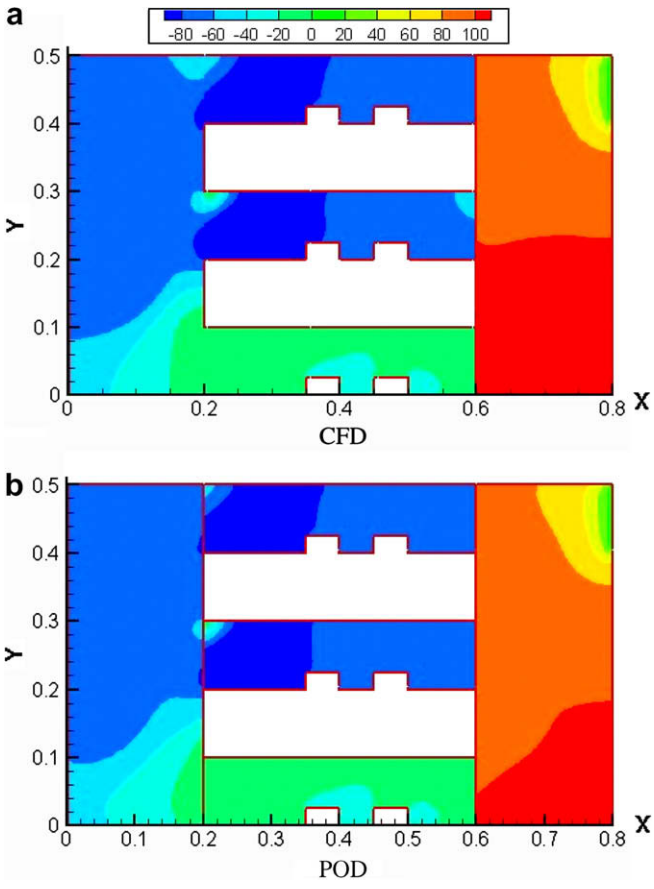

Fig. 11. Pressure (Pa) comparison at system level: (a) CFD and (b) POD.

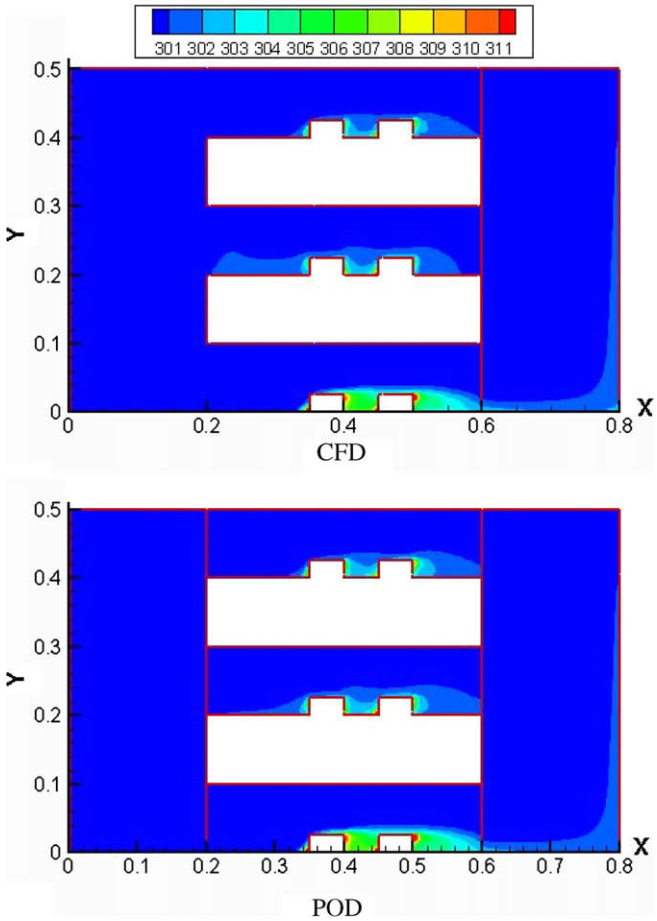

Fig. 12. Temperature (K) comparison at system level: (a) CFD and (b) POD.

To justify the accuracy of POD results, the following Euclidean *L2* error norm is defined:

$$V^{r}_{err} = \frac{||V^{r} - V^{t}||}{||V^{t}||} \tag{22}$$

where V represents velocity, pressure, and temperature rise over ambient temperature, respectively.

4.1. Component level simulation

The velocity modal spectra for the three models for representative test case shown in Tables 1–3 are plotted in Fig. 5a, which indicates that the first modes dominate the system energy. It should be noted that the cases $k = 1$–6 in Tables 1–3 are used for snapshots and the case k = test is for the verification of POD modeling. The plenum model contained 4141 grid cells, or 24,846 total DOF to model the flow considering u, v, P, T, k, ε are solved for in each grid cell, while the reduced order model contains only $6 \times 3 = 18$ DOF, for an $O(10^3)$ reduction in DOF. Similarly, an $O(10^3)$ reduction in DOF can be achieved for server and exhaust plenum models. The *L2* error norm for the velocity field showed that the boundary conditions were satisfied with 3% and velocity approximation error was 3.5%. Fig. 6 compares the velocity fields obtained by both CFD and POD simulations for the three sub-domain models. Close agreement is achieved between the true and approximate solutions, both within the field and at the boundary. The approximations of pressure fields for the three ROMs of the example

considered are shown in Fig. 7, which are also in good agreement with the CFD simulations.

Fig. 5b plots the temperature modal spectra, and Fig. 8 illustrates the temperature fields for server 2 and exhaust plenum models with POD and CFD, respectively. It is noted that only partial range of temperatures is shown for the server model for improved visualization. Using the first single mode, the POD method has a $L2$ error norm of less than 7.4% for server 2. The largest errors occur near the surface of the blocks where the largest temperature gradients occur. The primary reason that temperature has larger error than the velocity and pressure is that the total heat flow rate, instead of the heat flux at each surface of the heating block is matched. In contrast, fluid flow rate is matched at a single interface such as inlet or outlet, which generates better approximation. Another possible reason is that the error of flow field may propagate to the temperature field. Table 4 summarizes the POD modeling errors for each component for representative test case shown in Tables 1–3.

4.2. System level simulation

The system level model is constructed by connecting the three server ROMs and the intake and exhaust plena ROMs together. Induced fan models are placed at the outlet of the server models to drive the system flow. The inlet and outlet pressures to the system can be assumed to be zero without loss of generality. A cubic pressure–velocity relationship is used for the fan model

$$\Delta P(u) = 200 - 40u + 20u^2 - 4u^3 \tag{23}$$

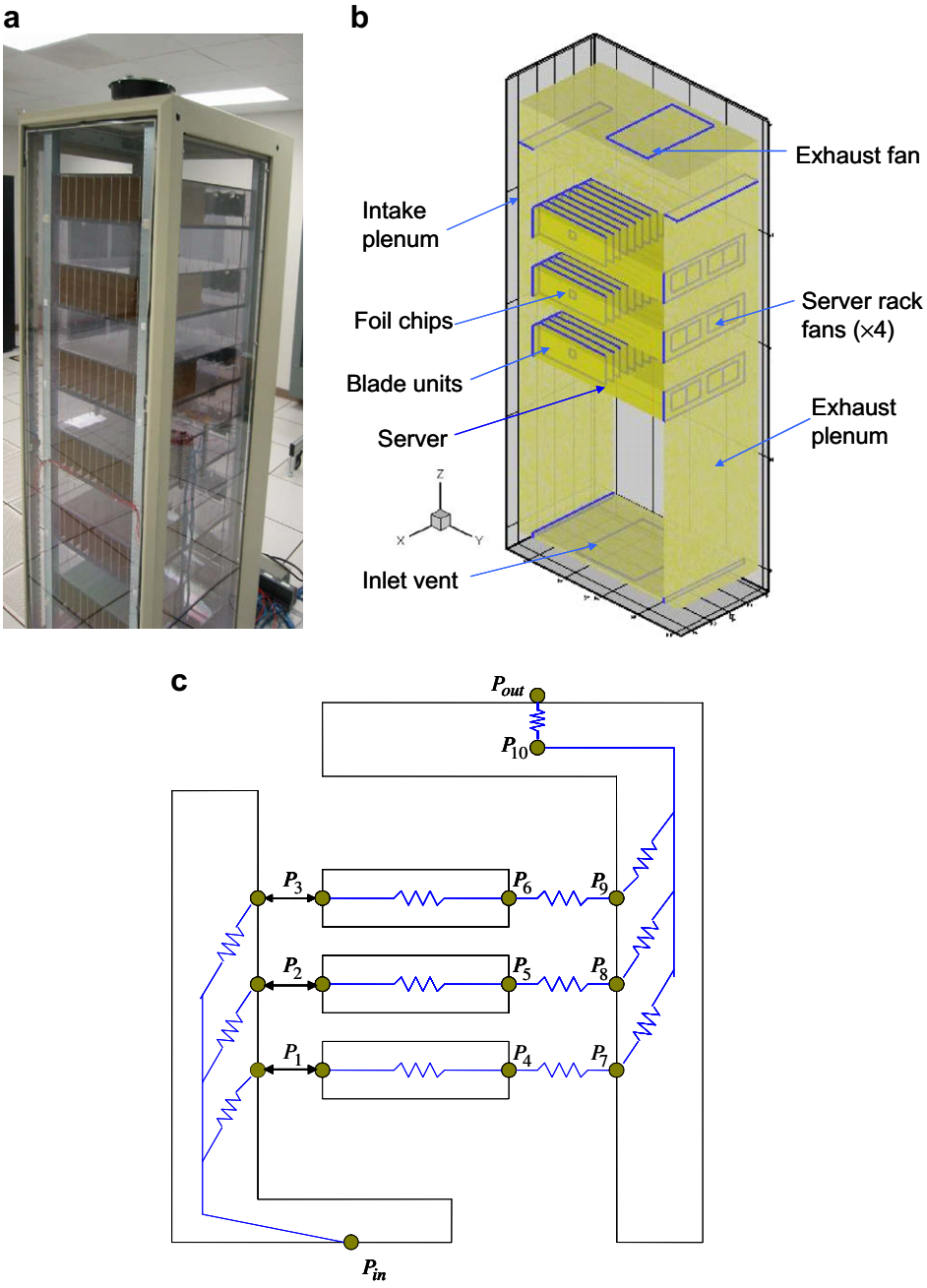

Fig. 13. Simulated rack: (a) experimental model and (b) numerical model, and (c) system flow resistance network.

Table 6
Simulated rack geometry and properties

Blade server unit length	0.44 (m)
Blade server unit gap	0.4 (m)
Bottom bay height	0.20 (m)
Foil chip size	0.32 × 0.32 (m) × (m)
Plenum depth	0.072 (m)
Rack depth	0.864 (m)
Rack height	2.00 (m)
Rack width	0.512 (m)
Rack inlet width	0.36 (m)
Rack inlet length	0.32 (m)
Rack exit bay	0.182 (m)
Rack exhaust fan diameter	0.15 (m)
Server width	0.44 (m)
Server depth	0.72 (m)
Server height	0.132 (m)
Foil chip thermal conductivity	387.6 (W/m K)
FR4 PCB thermal conductivity [2]	
In plane	0.204 (W/m K)
Lateral	9.074

where the area-averaged velocity u at the horizontal direction is based on the control volumes at the interface. The system nomenclature and flow network are illustrated in Fig. 9. It is noted that each component sub-domain is identified with a superscript as Ω^j, $j = 1,2,\ldots,5$ and the mass or heat flux at the kth control surface (interface) for the jth sub-domain as $G^{j,k}$. The heat loads for the chips within server 1, server 2, and server 3 are 110 W, 110 W, and 90 W, respectively. A zero gauge pressure is set at both inlet and outlet of the cabinet.

The pressure loss coefficients K_1, K_2 described in Eq. (9) for each component are summarized in Table 5 along with the r^2 values. The pressure drop characteristic of intake and exhaust plena models shown in Table 5 may only work for the cases where all connected servers have the same fan settings (many commercial server cabinets indeed have the same fan setting for each server). More snapshots may be needed for more complicated pressure characteristics.

The FNM simulation showed that a relative error for the approximate link mass flow rates over all interfaces was within 4.5% and an error less than 3.9% for nodal pressure over pressure nodes P_1 to P_9. Figs. 10–12 plot the full CFD and approximate velocity, pressure and temperature fields, respectively. The FNM-POD simulations show good agreement with CFD simulations and good continuity at the interfaces of sub-domains, which was a problem when no boundary profile is considered. The $L2$ error norm is less than 12% for all models, with the largest error occurring at the leading and trailing edges (recirculation regions) of servers and the

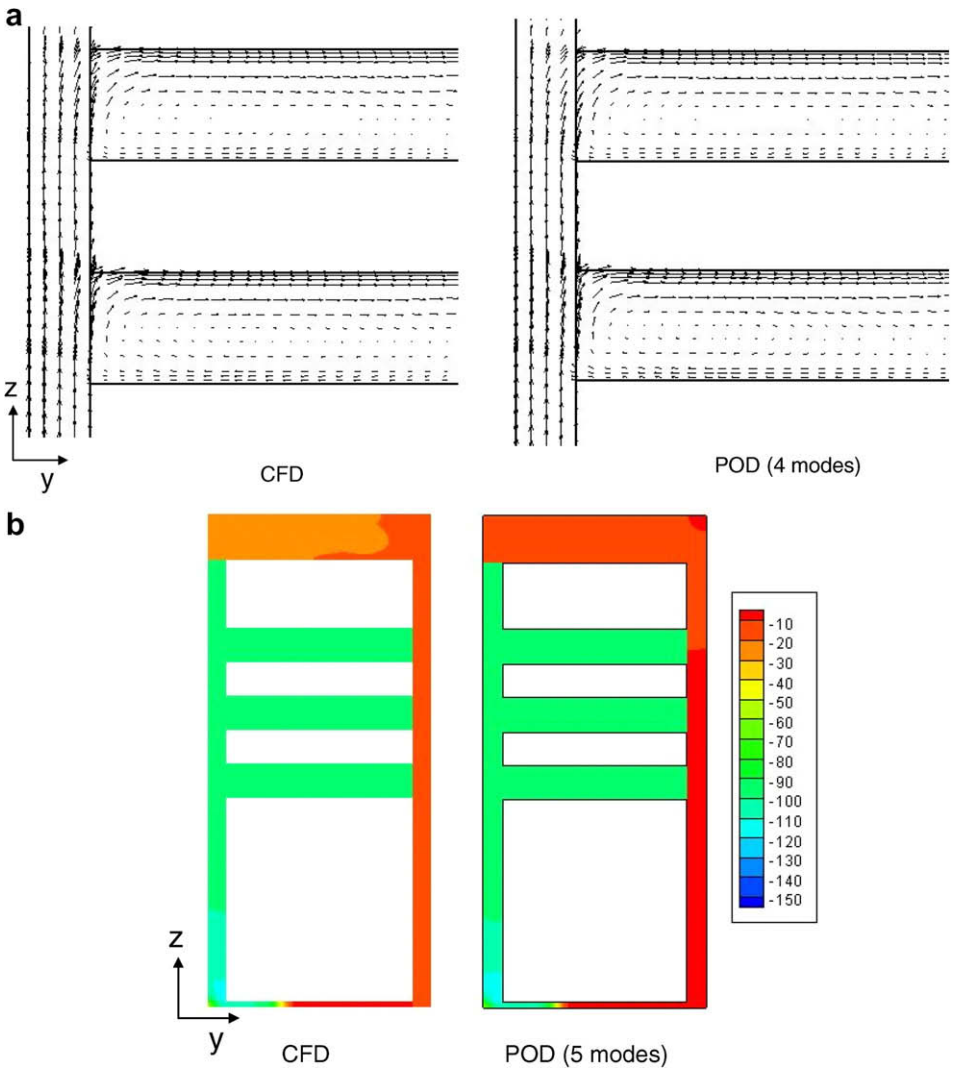

Fig. 14. Comparison of CFD and FNM-POD simulation results at system level for simulated rack: (a) velocity field and (b) pressure field (Pa).

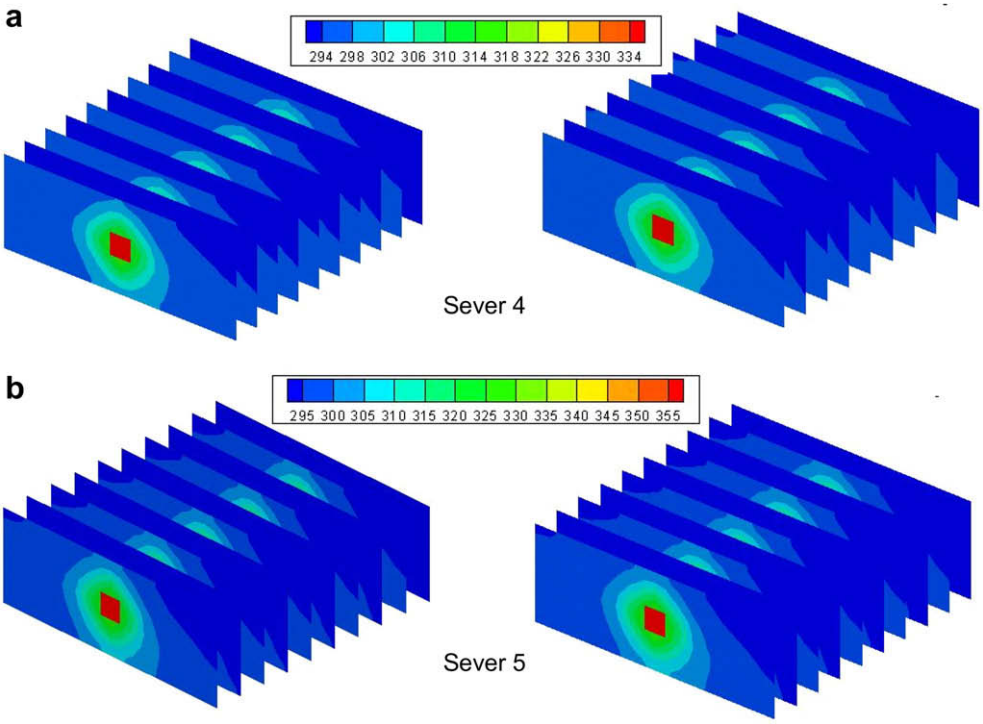

Fig. 15. Comparison of CFD and FNM-POD simulation results for temperature distribution across chips and FR4 board at system level for simulated rack: (a) server 4 and (b) server 5.

exhaust plenum. Besides the errors associated with FNM and POD modeling itself, downstream feedback is not captured by this approach. Therefore, this approach may not be valid when strong recirculation occurs inside the system. To efficiently capture the downstream effects, an accurate boundary profile needs to be specified downstream, which is typically difficult. Although this profile can be approximated by adding an adjacent component, such as a duct in our case, there is still an error associated with this approximation. These errors contribute to the existing mismatch at the interfaces. The large error in the leading and trailing edges of servers, where the recirculation occurs, will not affect the high heat flux regions (i.e. the chips) significantly, since the velocities in those regions are relatively small and the general flow pattern across high heat flux regions is captured by this method. A much smaller error of 7% for the chip maximum temperatures has been achieved with this FNM-POD modeling approach. Another concern in connecting component models is the propagation of error and the accumulation of errors as more components are added to the system. Generally, the connection of components in parallel may not accumulate the modeling errors, but a connection in series may do so. However, FNM-POD based ROMs may limit the accumulation of this error because the individual models satisfy overall mass and energy balances. As illustrated earlier, an $O(10^3)$ reduction in DOF was achieved for each ROM, then the system ROM has an $O(10^3)$ reduction in DOF.

5. Experimental validation

The system studied in this investigation is a simulated blade server cabinet, whose schematic is shown in Fig. 13a [2]. This server cabinet is cooled using vertically oriented air flow distributed to seven servers with each server containing 10 blade units. Alternating server spaces are filled with blank units to block the airflow. For the demonstration, only servers 4, 5 and 6 are tested in both the numerical modeling and experiments. The complete cabinet

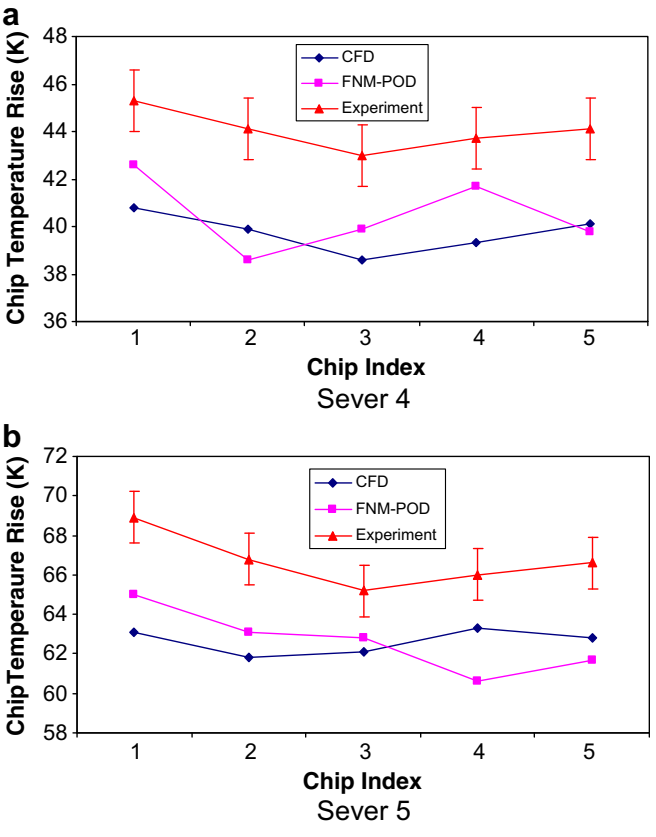

Fig. 16. Chip junction excess temperature comparison of CFD simulation, POD simulation, and measurement results at system level for mock rack (K): (a) server 4 and (b) server 5.

measures 0.6 m wide by 0.8 m deep by 2 m tall. Other geometric features and thermal properties are shown in Table 6. The overall flow through the cabinet is provided by a maximum of 0.108 m^3/s (550 CFM) exhaust fan on the top of the cabinet and flow movement through the server racks is provided by four 0.015 m^3/s (20 CFM) maximum fans. The blade servers are represented by the channels formed using large pieces of printed wiring board with a foil heater in the center on one side simulating the chip as dividers. Only half of the heaters in servers 4 and 5 are turned on for the testing and modeling. The entire rack is divided into three parts: intake plenum, servers, and exhaust plenum as shown in Fig. 13b, and its corresponding flow network is shown in Fig. 13c.

The CFD and FNM-POD simulation results for velocity and pressure fields are shown in Fig. 14 and the results for temperature distributions across the chips and printed wiring board substrates of server 4 ($Q = 10$ W) and server 5 ($Q = 15$ W) are shown in Fig. 15. The CFD and FNM-POD simulations are compared with experiments for chip junction temperature rise over ambient temperature (293 K at a data center lab) in Fig. 16. The FNM-POD simulation results are seen close to the CFD simulation results, with a maximum relative error of 7.9%. Compared to the maximum error up to 15% in some regions (leading and trailing edges of server and exhaust models), the high heat flux regions (i.e. the chip areas) are more accurately predicted at the system level. The FNM-POD results are generally higher than the CFD results. One possible reason is that the duct attached to the intake model for the intake ROM development may not be long enough to fully transmit the flow across the connected server. A larger flow rate may go through the top region of servers, resulting in lower convection heat transfer at the chips, compared to the full CFD system level simulation. It can be seen that both FNM-POD and CFD results under-predict the chip junction temperatures with a maximum approximation error of 10%. This is because the real system flow resistance is higher than the numerical model due to the wiring and surface roughness. The contact thermal resistances between chips and thermocouples may also contribute to this discrepancy. The experimental uncertainty was estimated to be about ±1.2 K, which includes ±0.4 K for the T-type thermocouples and ±0.8 K for location and thermal resistance and power supply uncertainties [31]. The system model contained 258,720 grid cells or 1,811,040 total DOFs to model the flow considering u, v, w, P, T, k, ε are solved for in each grid cell, while the reduced order model has only 119 DOFs ($2 \times 7 = 14$ for flow resistance network, and a maximum of $7 \times 3 \times 5 = 105$ for POD), an $O(10^4)$ reduction in DOF is achieved.

6. Conclusion

A reduced order modeling methodology is developed for large-scale thermal system with pressure-driven flows. The complimentary POD method with flux matching technique is used to construct the ROM for each sub-system. To capture the effect of the inlet boundary profile on the domain of the system, the upstream output of the sub-system is used as the input to the adjacent sub-system down stream. A flow straightening duct may be necessary to better approximate the boundary profile of the air flow. To model the pressure field in incompressible flow, the surface-response method is considered in solving the weight coefficients of pressure POD modes. Flow network modeling was used to assemble various components, by coupling the pressure, mass and energy flow rates at the interface. To validate the simulation results of this methodology, experiments were conducted in a simulated rack containing five blade servers.

The results indicate acceptable approximations are possible from this methodology to simulate the behavior of a larger system comprised of numerous sub-domains. The example presented here is characterized by the sub-domain interfaces located near swirling flow features such as the recirculation region near the trailing edge of the obstructions in the server models. Even with such limited ROM model behavior, the result systems-level model produces reasonably accurate representation of the thermal flow fields, while a reduction of several magnitudes of orders in DOF was achieved.

Acknowledgements

The authors acknowledge support for this research from the Office of Naval Research under Contract No. N00014-04-1-0335, monitored by Dr. Mark Spector. The authors also thank the reviewers for their valuable comments.

References

[1] J. Rambo, Reduced-Order Modeling of Multiscale Turbulent Convection: Application to Data Center Thermal Management, Ph.D. thesis, Georgia Institute of Technology, Atlanta, GA, 2006.
[2] N. Rolander, An Approach for the Robust Design of Air Cooled Data Center Server Cabinets, MSME thesis, Georgia Institute of Technology, Atlanta, GA, 2005.
[3] B. Shapiro, Creating reduced-order models for electronic systems: an overview and suggested use of existing model reduction and experimental system identification tools, IEEE Trans. Compon. Parts Manuf. Technol. 26 (1) (2003) 165–172.
[4] Z. Zuo, L.R. Hoover, Advanced thermal architecture for cooling of high power electronics, IEEE Trans. Compon. Pack. Technol. 25 (4) (2002) 629–634.
[5] P. Holmes, J.L. Lumley, G. Berkooz, Turbulence, Coherent Structures, Dynamical Systems and Symmetry, Cambridge University Press, Cambridge, Great Britain, 1996. pp. 86–127.
[6] A.E. Deane, I.G. Kevrekidis, G.E. Karniadakis, S.A. Orszag, Low-dimensional models for complex geometry flows: application to grooved channels and circular cylinders, Phys. Fluids A 3 (10) (1991) 2337–2354.
[7] B. Galletti, C.H. Bruneau, L. Zannetti, A. Iollo, Low-order modeling of laminar flow regimes past a confined square cylinder, J. Fluid Mech. 503 (2004) 161–170.
[8] X. Ma, G.E. Karniadakis, A low-dimensional model for simulating three-dimensional cylinder flows, J. Fluid Mech. 458 (2002) 181–190.
[9] H.M. Park, D.H. Cho, Low dimensional modeling of flow reactors, Int. J. Heat Mass Transfer 39 (16) (1996) 3311–3323.
[10] L. Sirovich, Turbulence and dynamics of coherent structures, Parts I–III, Quart. Appl. Math. XLV (3) (1987) 561–590.
[11] E. Arian, M. Fahl, E.W. Sachs, Trust-region Proper Orthogonal Decomposition for Flow Control, ICASE Report, NAS1-97046, Langley Research Center, Hampton, VA, May 2000.
[12] H.M. Park, O.Y. Kim, Reduction of modes for the control of viscous flows, Int. J. Eng. Sci. 39 (2001) 177–200.
[13] H.M. Park, W.S. Jung, The Karhunen–Loeve Galerkin Method for the inverse natural convection problems, Int. J. Heat Mass Transfer 44 (1) (2001) 155–167.
[14] S.S. Ravindran, A reduced order approach to optimal control of fluids using proper orthogonal decomposition, Int. J. Numer. Meth. Fluids 34 (5) (2000) 425–448.
[15] S.S. Ravindran, Adaptive reduced-order controllers for a thermal flow using proper orthogonal decomposition, SIAM J. Sci. Comput. 23 (6) (2002) 1924–1942.
[16] S.S. Ravindran, Control of flow separation over a forward-facing step by model reduction, Comput. Meth. Appl. Mech. Eng. 191 (41) (2002) 4599–4617.
[17] B.H. Jorgensen, J.N. Sorensen, M. Brons, Low-dimensional modeling of a driven cavity flow with two free parameters, Theor. Comput. Fluid Dyn. 16 (2003) 299–317.
[18] D. Rempfer, On low-dimensional Galerkin Models for fluid flow, Theor. Comput. Fluid Dyn. 14 (2) (2000) 75–88.
[19] H.V. Ly, H.T. Tran, Modeling and control of physical processes using proper orthogonal decomposition, Math. Comput. Model. 33 (2001) 223–236.
[20] C.W. Rowley, T. Colonius, R.M. Murray, Model reduction for compressible flows using pod and Galerkin projection, Physica D 189 (2004) 115–129.
[21] Y. Utturkar, B. Zhang, W. Shyy, Reduced-order description of fluid flow with moving boundaries by proper orthogonal decomposition, Int. J. Heat Fluid Flow 26 (2005) 276–288.
[22] J. Rambo, Y. Joshi, Reduced order modeling of steady turbulent flows using the POD, in: ASME Summer Heat Transfer Conference, San Francisco, CA, 2005.
[23] J. Rambo, Y. Joshi, Reduced-order modeling of turbulent forced convection with parametric conditions, Int. J. Heat Mass Transfer 50 (3-4) (2007) 539–551.
[24] T. Kowalski, A. Radmehr, Thermal analysis of an electronics enclosure: coupling flow network modeling (FNM) and computational fluid dynamics (CFD), in: IEEE 16th Semiconductor Thermal Measurement and Management Symposium, San Jose, CA, 2000, pp. 60–67.

[25] C. Belady, K.M. Kelkar, S.V. Patankar, Improving productivity in electronic packaging with flow network modeling (FNM), Electron. Cooling 5 (1) (1995) 36–40.
[26] B. Lian, T. Dishongh, D. Pullen, H. Yan, J. Chen, Flow network modeling for improving flow distribution of microelectronics burn-in-oven, in: The 7th Intersociety Conference on Thermal and Mechanical Phenomena in Electronic Systems, Las Vegas, NV, 2000, pp. 81–91.
[27] B. Kader, Temperature and concentration profiles in fully turbulent boundary layers, Int. J. Heat Mass Transfer 24 (9) (1981) 1541–1544.
[28] E.A. Christensen, M. Brons, J.N. Sorensen, Evaluation of proper orthogonal decomposition – based techniques applied to parameter dependent nonturbulent flows, SIAM J. Sci. Comput. 21 (4) (2000) 1419–1434.
[29] I.E. Idelchik, Handbook of Hydraulic Resistance, CRC Press, Florida, 1994. pp. 8.1–8.30.
[30] S.V. Patankar, Numerical Heat Transfer and Fluid Flow, MacGraw Hill, New York, 1980. pp. 121–135.
[31] X. Wei, Stacked Microchannel Heat Sinks for Liquid Cooling of Microelectronics Devices, Ph.D. thesis, Georgia Institute of Technology, Atlanta, GA, 2004.